"Super-parameterization": A better way to simulate regional extreme precipitation?

Fuyu Li,[1] Daniele Rosa,[2] William D. Collins,[1,2] and Michael F. Wehner[3]

Received 1 November 2011; accepted 8 February 2012; published 4 April 2012.

[1] Extreme precipitation is generally underestimated by current climate models relative to observations of present-day rainfall distributions. Possible causes of this systematic error include the convective parameterization in these models that have been designed to reproduce measurements of climatological mean precipitation. One possible approach to improve the interaction of subgrid-scale physical processes and large-scale climate is to replace the conventional convective parameterizations with a high-resolution cloud-system resolving model. A "super-parameterized" Community Atmosphere Model (SP-CAM) utilizing this approach is used in this study to investigate the distribution of extreme precipitation in the United States. Results show that SP-CAM better simulates the distributions of both light and intense precipitation compared to the standard version of CAM based upon conventional parameterizations. The improvements are mostly seen in regions dominated by convective precipitation, suggesting that super-parameterization provides a better representation of subgrid convective processes.

Citation: Li, F., D. Rosa, W. D. Collins, and M. F. Wehner (2012), "Super-parameterization": A better way to simulate regional extreme precipitation? *J. Adv. Model. Earth Syst.*, *4*, M04002, doi:10.1029/2011MS000106.

1. Introduction

[2] Extreme precipitation events often have dramatic ecological, economic, and sociological impacts. The simulation and projection of precipitation extremes are of great importance as significant upward trends in the frequency of these events have been detected in recent decades with the warming of the climate [*Min et al.*, 2009, 2011], and further increases could affect less resilient sectors of society and the environment [*Schneider et al.*, 2007]. Despite the need for robust projections, it has been repeatedly demonstrated that current climate models generally underestimate the occurrence of intense precipitation as reported in several recent studies [e.g., *Durman et al.*, 2001; *Boyle and Klein*, 2010; *Li et al.*, 2011a].

[3] The relatively coarse horizontal resolution typical of previous generations of climate models has been proposed as the main reason for the underestimation of extreme precipitation. Recent studies [e.g., *Chen and Knutson*, 2008; *Wehner et al.*, 2010] have suggested that low-resolution climate models, particularly those with grid spacings of 1° or more, cannot reproduce the statistics of extreme rainfall events in the historical climate record with sufficient fidelity. Although increases in resolution yield more realistic spatial patterns and probability distributions of precipitation over most continental regions [*Boyle and Klein*, 2010], the systematic errors in these properties persist during convective-precipitation dominated seasons, e.g., June-July-August (JJA) and March-April-May (MAM), in the southeast USA [*Iorio et al.*, 2004]. This result is consistent with the finding that convective precipitation appears to decrease while total precipitation appears to increase with greater horizontal resolution [*Williamson*, 2008; *Li et al.*, 2011b]. Therefore, while the scale separation between convective and large-scale precipitation is a reasonable approximation in low-resolution models, increasing the resolution does not necessarily ensure an accurate simulation of convective precipitation. The reason is that the scale-separation approximation introduced in most parameterizations becomes less accurate as the model resolution approaches the scales of individual convective systems.

[4] A promising approach to improve the representation of subgrid-scale physical processes in climate models is to replace the conventional cloud parameterizations with a high-resolution cloud-resolving model (CRM) embedded into each model grid column. This technique is often designated by "super-parameterization" (SP) [e.g., *Khairoutdinov and Randall*, 2001; *Khairoutdinov et al.*, 2005]. In comparison to conventional parameterizations, SP is conjectured to improve

[1]Earth Sciences Division, Lawrence Berkeley National Laboratory, Berkeley, California, USA.
[2]Department of Earth and Planetary Science, University of California, Berkeley, California, USA.
[3]Computational Research Division, Lawrence Berkeley National Laboratory, Berkeley, California, USA.

1942-2466/12/2011MS000106

the representation of sub-grid processes since the embedded CRMs can explicitly resolve the interactions among cloud dynamics, cloud and aerosol microphysics, radiation, and turbulence down to cloud-system scales. SP can dramatically improve the diurnal cycle of precipitation over summertime continents [*Khairoutdinov et al.*, 2005] while it simultaneously produces reasonable simulations of time-mean precipitation. *Iorio et al.* [2004] further showed that a climate model (CCM3) enhanced using the SP methodology can produce longer tails of the precipitation distribution over the continental United States (CONUS), and *DeMott et al.* [2007] indicated that a similar approach can simulate intense rainfall events more correctly.

[5] This study will specifically investigate how the SP approach can be used to simulate the extreme precipitation over the CONUS compared with precipitation produced using a climate model with conventional parameterizations. We focus on the CONUS because of the extensive rain gauge data, which, when appropriately gridded, can be readily used in the comparison. Section 2 presents the description of model framework and the observational precipitation data used to evaluate the conventional and SP-based climate-model simulations. The results are presented in section 3 and conclusions are discussed in section 4.

2. Model and Data Description

2.1. Model Description

[6] We use the National Center for Atmospheric Research (NCAR) Community Atmosphere Model (CAM) version 3.5.36 as the main modeling framework [*Collins et al.*, 2006]. For our simulations, we have selected CAM with a finite-volume dynamical core configured with a horizontal resolution of 1.875° latitude $\times$ 2.5° longitude and 28 vertical levels. At this lateral resolution the model is integrated forward in time using time steps of 30 minutes, and the state of the model is output every 3 hours to capture short-lived hydrometeorological events. Two simulations are performed to investigate the performance of SP in simulating extreme precipitation relative to conventional approaches: (1) CAM with standard parameterizations of cloud and convection processes [*Collins et al.*, 2004]; and (2) "super-parameterized" CAM (SP-CAM), with a CRM embedded in each grid cell in place of these standard parameterizations [*Khairoutdinov and Randall*, 2001].

[7] Details of the configurations of the two simulations have been described by D. Rosa et al. (Global transport of passive tracers in conventional and super-parameterized climate models: Evaluation of multiscale methods, submitted to *Journal of Advances in Modeling Earth Systems*, 2012). The most important aspect is that both simulations have been performed in "chemical transport" mode, in which CAM fields are replaced by equivalent fields from the NCEP Re-analysis including horizontal winds, temperature, surface pressure, wind stress, sensible heat flux and water vapor flux. This mode of operation insures that the large-scale fields in CAM are fully consistent with a reanalysis for the actual meteorological conditions pertaining to our time series of rain gauge data. These dynamic and thermodynamic fields are linearly interpolated in time to the CAM time step and interpolated in space onto the CAM grid. The CRM embedded in each atmospheric column of CAM is nudged to CAM large-scale fields using relaxation terms [*Khairoutdinov et al.*, 2005]. The difference in CAM-grid scale precipitation simulations is from the difference of sub-grid cloud and dynamical processes in the two simulations. Therefore to leading order, we hypothesize that differences between the modeled and observed extreme precipitation are due to systematic errors in the sub-grid physics rather than the large-scale meteorological fields.

[8] The CRM in SP-CAM is a configured as a 2D system with 2 km horizontal resolution. Each CRM domain consisting of 64 columns is aligned in the west-east direction and exchanges information with itself via periodic lateral boundary conditions. Its vertical grid levels are located at the same heights as the 28 levels of CAM. The CRM solves the non-hydrostatic momentum equations with an anelastic approximation (detailed by *Khairoutdinov and Randall*, [2001]). A bulk microphysics parameterization is used to compute the hydrometeor conversion rates and terminal velocities. The prognostic thermodynamic variables including the water moist static energy and precipitating water are used to calculate the cloud water, cloud ice, rain, snow and graupel mixing ratios.

[9] The 2-km CRM horizontal resolution is chosen to optimally balance the computational cost and realistic simulation of the formation of the cloud and extreme precipitation. *Ooyama* [2001] showed that 2-km resolution is needed for realistic simulations of precipitating clouds using a 2D non-hydrostatic model, which is in many ways similar to the embedded CRM used in this framework. His tests on the growth of single cell clouds showed that, at 2-km resolution, the rain has more realistic and clearer episodes with the peak rain intensity doubling that in the coarser 4-km experiment, which only produces very gentle and continuous precipitation. Although more complex cloud structure and greater precipitation intensity are seen in 1-km experiment, the 2-km resolution captures the rain episodes and peak intensities reasonably well. These results provide a solid proof of using the 2-km CRM in the SP-CAM framework when taking into account the computation cost. Meanwhile, *Ooyama* [2001] also indicates that increasing the CRM's resolution in the SP-CAM could slightly increase the intensity of extreme precipitation. It may be worth future investigation but the impact of the horizontal resolution of the CRM is not the focus of this framework.

[10] In CAM, the precipitation is parameterized through large-scale and convective precipitation schemes. The mass vertical fluxes are calculated based on the assumption that the cumulus ensemble depletes the convectively available potential energy on a fixed characteristic timescale. However in SP-CAM, each CRM is forced by the grid-scale tendencies from CAM

and it then computes the convective tendencies in each column in its domain. The SP-CAM framework thus includes both the large-scale atmospheric vertical motion on the climate model grid and the cloud-scale circulations represented on the CRM's grid [*Khairoutdinov et al.*, 2008]. Both scales of the vertical motions are involved in the formation of precipitation, but the conventional climate model parameterizes the distributions of cloud-scale velocities. *Khairoutdinov et al.* [2008] have shown that, despite the relatively coarse grid spacing of the CRM, the clouds simulated by the CRMs in SP-CAM behave in a manner consistent with our understanding of the stratocumulus dynamics, and that the bulk of vertical transport of water is carried out by the circulations explicitly represented on the CRM grid.

2.2. Precipitation Data

[11] We assess the performance of CAM and SP-CAM in simulating extreme precipitation using a rain gauge-based observational precipitation dataset from the NOAA Climate Prediction Center (CPC). The specific product we use is the daily U.S. Unified Precipitation product [*Higgins et al.*, 2000]. The dataset is derived from ~13000 rain gauge station reports collated each day since 1992 using three different data sources: NOAA's National Climate Data Center (NCDC) daily co-op stations, a CPC collation containing River Forecast Centers data first order stations, and daily accumulations from hourly precipitation measurements. The station daily-accumulated precipitation rates are mapped onto a regular $0.25^\circ \times 0.25^\circ$ grid for the U.S. continent using a Cressman Scheme [*Cressman*, 1959; *Charba et al.*, 1992] after application of quality controls to eliminate duplicative and overlapping stations [*Higgins et al.*, 2000]. The values are accumulated from noon of the day before to noon of each reported day. A ten year period of the gridded dataset spanning 1996 – 2005 that coincides with the simulation period is used to ensure internal consistency between the models and observations.

[12] Since extreme precipitation normally occurs on sub-daily time scales, we also analyze the simulations at 3-hourly intervals using the gridded hourly CPC precipitation [*Higgins et al.*, 2000]. The hourly precipitation is mapped onto a coarser 2×2.5 grid covering the contiguous United States using the same Cressman Scheme [*Cressman*, 1959; *Charba et al.*, 1992] that is applied to the daily data. The main difference between the daily and hourly gridded precipitation data is that most stations used for the daily product do not record hourly precipitation rates. One-third of the stations used for the hourly precipitation product are first order National Weather Service (NWS) stations, and the remaining stations consist of point measurements from cooperative observers. Since the set of hourly stations is a relatively small subset of the stations used in the daily precipitation product, some differences are expected in the gridded spatial distributions of time-mean precipitation rates. In addition, the hourly precipitation product is less up-to-date and covers only part of the simulation period from 1996–2001.

[13] To facilitate direct comparisons with the simulations, the daily and hourly gridded rain gauge precipitation rates have been regridded onto the CAM grid and outer (large-scale) SP-CAM grid using an area weighted interpolation scheme designed to conserve total precipitation. The 3-hourly model outputs are also averaged to daily values when compared to daily observations. Note that the intensities of some extreme precipitation events in the re-gridded data and/or daily data constructed from the 3-hourly data may be significantly reduced by the spatial interpolation and temporal averaging.

3. Results

3.1. Mean and Extreme Precipitation

[14] The time-mean distributions of precipitation over the CONUS region for CAM and SP-CAM are shown in Figures 1a and 1b, respectively. Since both CAM and SP-CAM are strongly constrained by NCEP reanalysis fields including surface moisture flux fields, the spatial patterns of CAM and SP-CAM are very similar as expected. Both simulations show high precipitation rates in the northwestern, eastern, and southeastern US. Relative to CAM, the precipitation is slightly higher in SP-CAM in these wet regions but a little lower in dry middle-west US. This difference implies some fundamental differences in the precipitation statistics between the two models that will be discussed in more detail below.

[15] CAM and SP-CAM generally have higher mean precipitation rates than CPC rain gauge precipitation over the CONUS region (Figure 1): ~30% higher for the region averaged mean daily precipitation (Table 1). The excess precipitation is primarily related to the differences between NCEP precipitation [*Kalnay et al.*, 1996] and CPC precipitation fields at large scales (Figures 1c, 1d, and 2) and to the underestimation of topographic effects from the Rocky Mountains due to the coarse spatial resolutions of the models. Over the eastern US, the maximum precipitation in CPC occurs in the states adjacent to the Gulf of Mexico, while the precipitation in CAM and SP-CAM peaks in the central and Mid-Atlantic States. In addition, due to the sparser sampling rain gauge stations, the CPC 3-hourly precipitation (Figure 1d) is generally lower than the CPC daily precipitation although the two datasets share similar spatial patterns.

[16] The similarity in the mean precipitation between CAM and SP-CAM is expected since we constrain both models with large-scale dynamic and thermodynamic fields from the NCEP reanalysis (Figure 2). However at the level of corresponding grid points from each model, the two representations of subgrid cloud and convective processes are free to operate very differently subject to the nearly identical boundary conditions imposed on both grid points. Our experiments are designed to assess if the embedded CRM can better resolve extreme precipitation within the CAM model grid compared to the conventional precipitation parameterizations when forced by the same realistic meteorological fields. We

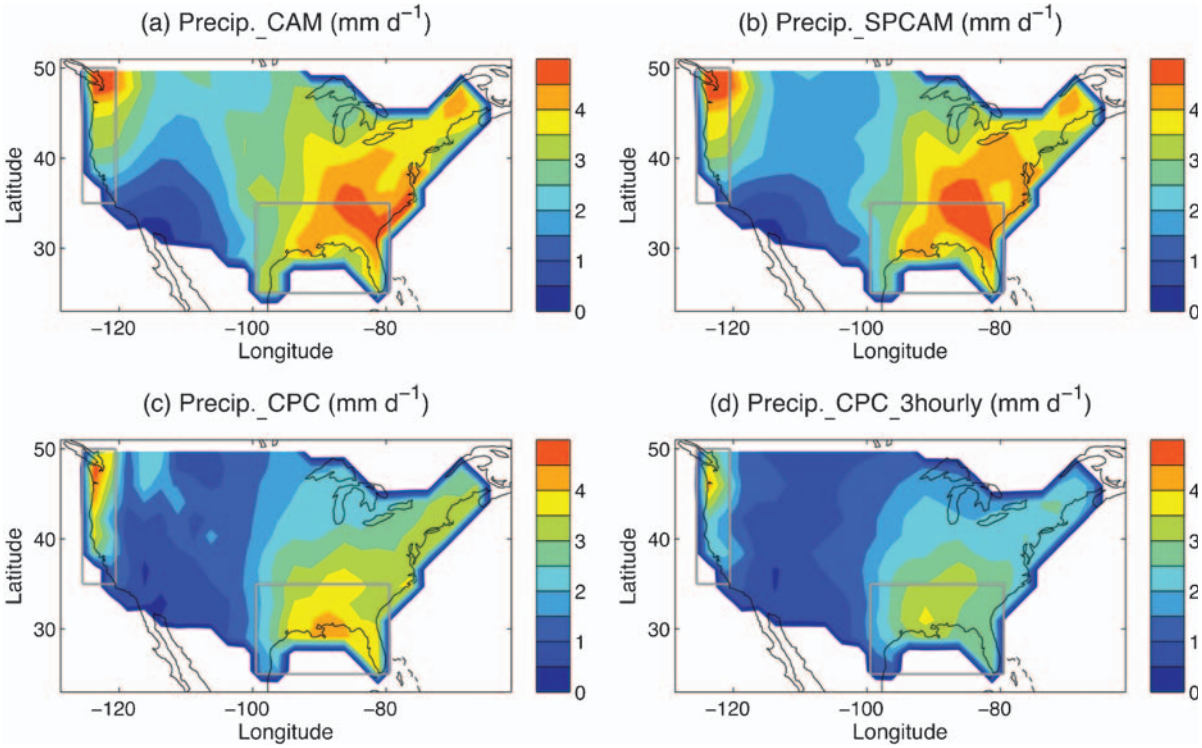

Figure 1. Mean precipitation for (a) CAM (1996–2005), (b) SP-CAM (1996–2005), (c) daily CPC (1996–2005), and (d) hourly CPC (1996–2001) on the same 1.875° latitude x 2.5° longitude model grid. Boxes denote the southeastern and western regions of the U.S. analyzed in section 3.

Table 1. The Mean, R95, and R995 Precipitation (mm d-1) From CAM, SPCAM and CPC, Averaged Over Three Regions: Continental U.S. (CONUS), Southeastern U.S. (SE) and Western U.S. (W)[a]

	Mean			R95			R955		
	CONUS	SE	W	CONUS	SE	W	CONUS	SE	W
CAM	2.9	3.8	3.4	18.5	24.2	22.7	45.8	61.7	50.3
SPCAM	2.8	3.7	3.7	22.7	30.1	26.7	60.8	81.4	54.2
CPC	2.2	3.3	3.0	20.1	32.2	25.2	61.7	89.0	56.7

[a]The SE U.S. and W U.S. are defined in section 3 (the two gray boxes in Figure 1).

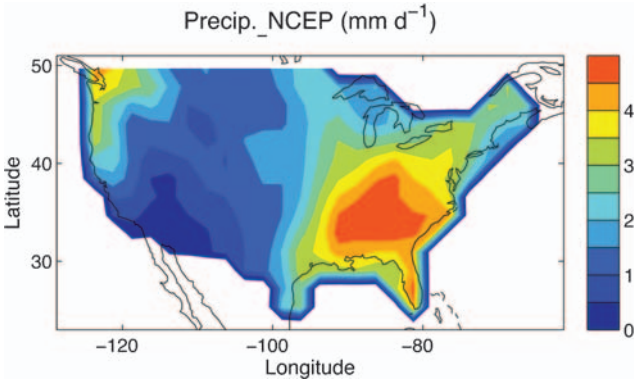

Figure 2. Mean precipitation from NCEP Re-analysis 6-hourly precipitation (1996–2005).

show the simulated and observed extreme precipitation in Figure 3 and their region averaged values in Table 1.

[17] The definitions of extreme precipitation used in this study are determined by high percentile thresholds applied to the daily and 3-hourly precipitation derived from the Frich indices with slight modifications [*Frich et al.*, 2002; *Alexander et al.*, 2006]. To facilitate our analysis, the units of the extreme precipitation indices have been converted from the yearly total extreme precipitation (mm yr^{-1}) to the daily-mean intensity of the extreme events (mm d^{-1}). We first find the value for the *n*th percentile precipitation during all the wet events (>1 mm d^{-1}) at the same location for a whole year. The extreme precipitation index R*n* is defined as the mean precipitation intensity for all the extreme events larger than the *n*th percentile value. We choose R95 (rates exceeding the 95th percentile value) for daily precipitation and R995 (rates exceeding the 99.5th percentile

value) for 3-hourly precipitation to have enough samples (~10–20 events per year) for robust statistics.

[18] The R95 daily extreme precipitation is shown in Figure 3a for CAM, Figure 3c for SP-CAM, and Figure 3e for CPC observations. The extreme precipitation simulated by SP-CAM is significantly higher than that in CAM although the spatial distributions of mean precipitation appear to be very similar (Figures 1a and 1b). SP-CAM simulates more extreme precipitation over almost the entire CONUS region, particularly in southeastern and western coastal US. While CAM exhibits a characteristic underestimation of extreme precipitation (Figures 3a and 3c) as noted in many previous studies [e.g., *Boyle and Klein*, 2010; *Li et al.*, 2011a], the spatial distribution and intensity of the extreme precipitation in SP-CAM much better matches the extreme precipitation derived from CPC rain gauge observations. For instance, the region averaged R95 precipitation over southeastern (SE) U.S. in CAM is ~25% lower than that in CPC, while the R95 from SP-CAM is only ~7% lower (Table 1). While the changes in precipitation from CAM to SP-CAM represent an improvement over much of the CONUS region, SP-CAM does not capture some of the very extreme values along the southeastern and eastern coasts and it overestimates extreme precipitation over dry western mountainous regions.

[19] Although the CPC daily precipitation is deemed more reliable because of the larger number of rain gauge stations used to construct it and the longer duration of the data record, the 3-hourly data may yield additional information at the sub-diurnal time scales most relevant to extreme precipitation. Figures 3b, 3d, and 3f show the spatial distributions of the R995 (> 99.5th percentile) extreme precipitation estimated using the 3-hourly CAM and SP-CAM output and CPC data set, respectively. Similarly to the daily extreme precipitation, the conventionally parameterized CAM greatly underestimates this measure of extreme precipitation while SP-CAM agrees much better with the CPC observations (also see Table 1), particularly in the eastern CONUS. SP-CAM still misses some very extreme precipitation events such as those in Texas, but its general spatial

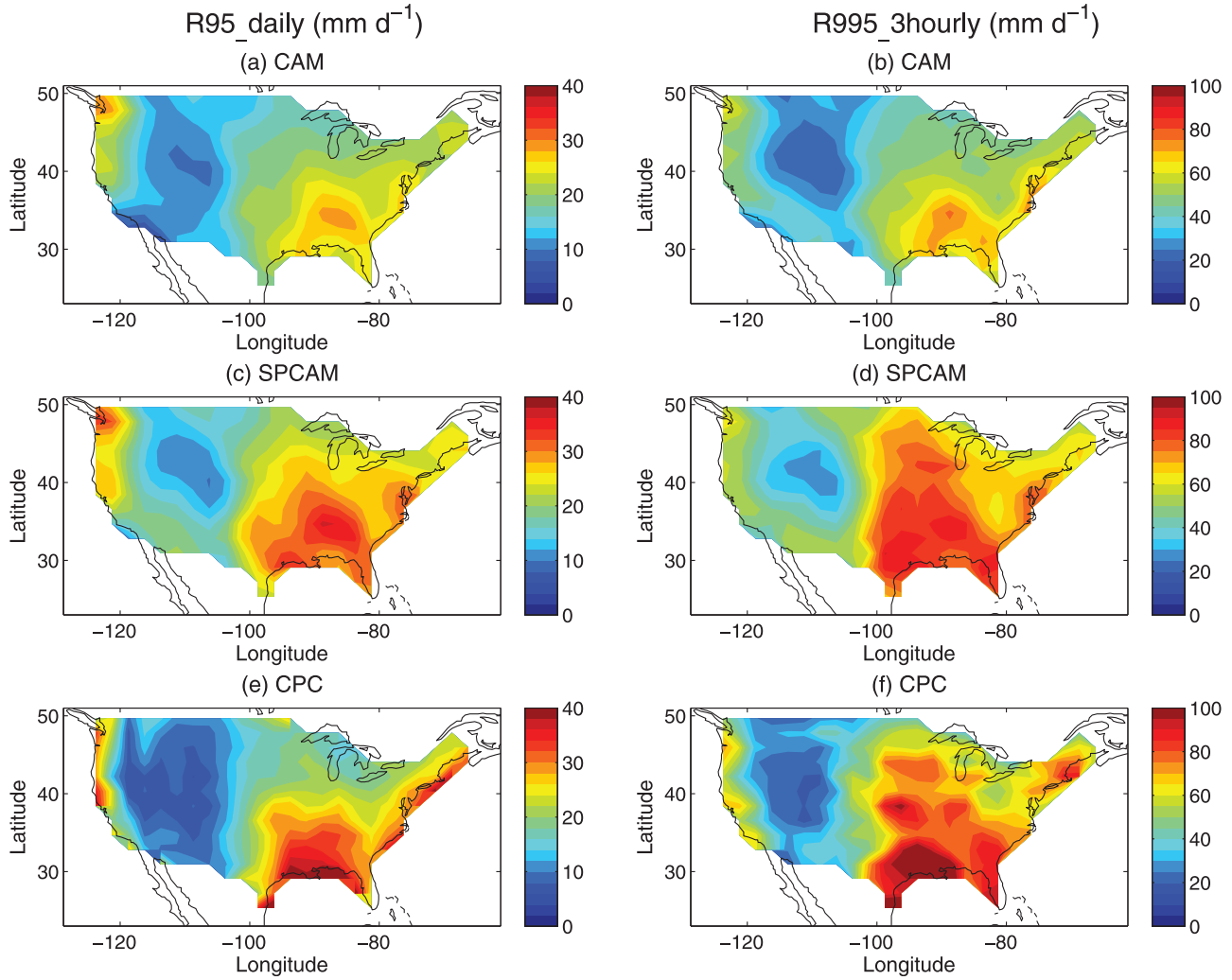

Figure 3. Simulated and observed U.S. extreme precipitation: 95th percentile daily precipitation for (a) CAM, (c) SP-CAM, (e) CPC; and 99.5th percentile 3-hourly precipitation for (b) CAM, (d) SP-CAM, (f) CPC.

patterns agree quite well with the CPC data. In general, the differences between CAM and SP-CAM (and between CAM and CPC) at 3-hourly time scales are much larger than those for daily extreme precipitation. This larger bias of CAM in 3-hourly extreme precipitation is expected due to the higher percentile threshold used which decreases the sample size and due to the shorter time scale which will be discussed in the next section.

3.2. Probability Distribution

[20] The results above show that SAM and SP-CAM produce similar spatial patterns of mean precipitation but produce quite different patterns and intensities of extreme precipitation. The difference indicates a shift of precipitation probability distributions towards higher extremes in SP-CAM relative to CAM. Figure 4 thus shows the probability density distribution of precipitation for CAM, SP-CAM and CPC. In addition to the whole CONUS region, we also analyze two sub-regions with high extreme precipitation: the southeastern U.S. between 25–35°N and 80–100°E and the western U.S. between 35–50°N and 55–60°E, defined as the two gray boxes in Figure 1. The precipitation is aggregated in 2 mm d^{-1} bins from 0 to 120 mm d^{-1}. Any precipitation rates larger than 120 mm d^{-1} are assigned to the last bin.

[21] Figure 4a shows the probability distribution for the daily precipitation over the CONUS region. CAM exhibits its characteristic underestimation of precipitation for heavy precipitation larger than 30 mm d^{-1}. The precipitation distributions from SP-CAM are generally in better agreement with the CPC observations particularly since SP-CAM simulates more light precipitation ($<$10 mm d^{-1}) and more heavy precipitation ($>$30 mm d^{-1}) than CAM. However, the frequency of the daily extreme precipitation from SP-CAM degrades at rates exceeding 60 mm d^{-1} and is comparable to that in CAM. The precipitation distribution over the southeastern U.S. (Figure 4c) is generally similar to that over the CONUS region (Figure 4a). The probability distributions from SP-CAM and CPC are in better agreement over the southeastern US, while CAM underestimates the probability of precipitation for rates exceeding $\sim$15 mm d^{-1}. Over the western coastal US, the probability distributions from both CAM and SP-CAM are in much better agreement with the CPC distribution (Figure 4e). However, the much larger area of the southeastern region relative to the western coastal zone implies that the distributions of extreme rainfall exceeding 30 mm d^{-1} are determined primarily by the southeastern region.

[22] In order to evaluate the simulation of sub-diurnal extreme events, the probability distributions of 3-hourly precipitation have been constructed as shown in Figures 4b, 4d, and 4f for the CONUS, southeastern US, and western US, respectively. Note that daily-mean precipitation rates calculated from diurnally averages of the 3-hourly dataset are not the same as the published CPC daily precipitation dataset. The reason is that the CPC 3-hourly precipitation dataset is derived from a subset of the daily rain gauge stations for just the first half of the daily dataset record, For consistency with the 3-hourly observations, the CAM and SP-CAM precipitation statistics shown here correspond to just 1996 – 2001 rather than the whole 10 year period for daily precipitation.

[23] The 3-hourly distributions show more extreme high and low precipitation rates compared to the daily distribution, as the daily temporal averaging eliminates the most extreme values. Over the entire CONUS region and southeastern US, the similarities and differences among the distributions of precipitation from CAM, SP-CAM, and CPC resemble those obtained in the comparisons of the daily data. For both the CONUS region and southeastern US, CAM overestimates the probability of moderate precipitation and underestimates the probability the heavy precipitation relative to CPC (Figures 4b and 4d). The SP-CAM distribution is in good agreement with that of CPC in conditions of light and heavy precipitation, although SP-CAM does overestimate the likelihood of moderate precipitation. The difference between CAM and SP-CAM is small over western U.S. apparently due to the relative frequency of various types of precipitation characteristic of this region. This feature is discussed in the next section.

3.3. Seasonal Variation of Probability Distribution

[24] The precipitation in CAM is parameterized as two separate processes representing convective and large-scale precipitation. In the real world, convective processes are more important in the southeastern U.S. than in the western coastal region where large-scale air motions (e.g., synoptic-scale frontal systems) are the principal driving mechanism for precipitation. The notable improvement in the simulation of the extreme precipitation distribution by SP-CAM in the southeastern U.S. is therefore likely due to the improved representation of subgrid convective processes in the CRMs embedded in SP-CAM. Similarly, the resemblance between CAM and SP-CAM over the western U.S. (Figure 4) should be expected because large scale air motions are prescribed when running in Chemical Transport Mode and therefore both models provide identical conditions for the formation of large-scale precipitation. Consequently, the seasonal variation of precipitation should also be improved as convective processes dominate summer precipitation over much of the CONUS.

[25] Figure 5 shows probability distribution of U.S. precipitation in JJA (Figures 4a and 4b) and in DJF (Figures 4c and 4d). For the convectively dominated summertime daily precipitation (Figure 5a), SP-CAM clearly simulates a much better distribution than CAM although it is still unable to capture the most extreme precipitation observed by CPC. CAM's underestimation of the high rain-rate tail of the precipitation distribution is more obvious in summer (JJA) than in the annual total (Figure 4a). The wintertime (DJF) difference between CAM and SP-CAM is much smaller than that in summer, reflecting the diminished importance of convective processes during this season. At the 3-hourly time scales, these differences are even more robust and

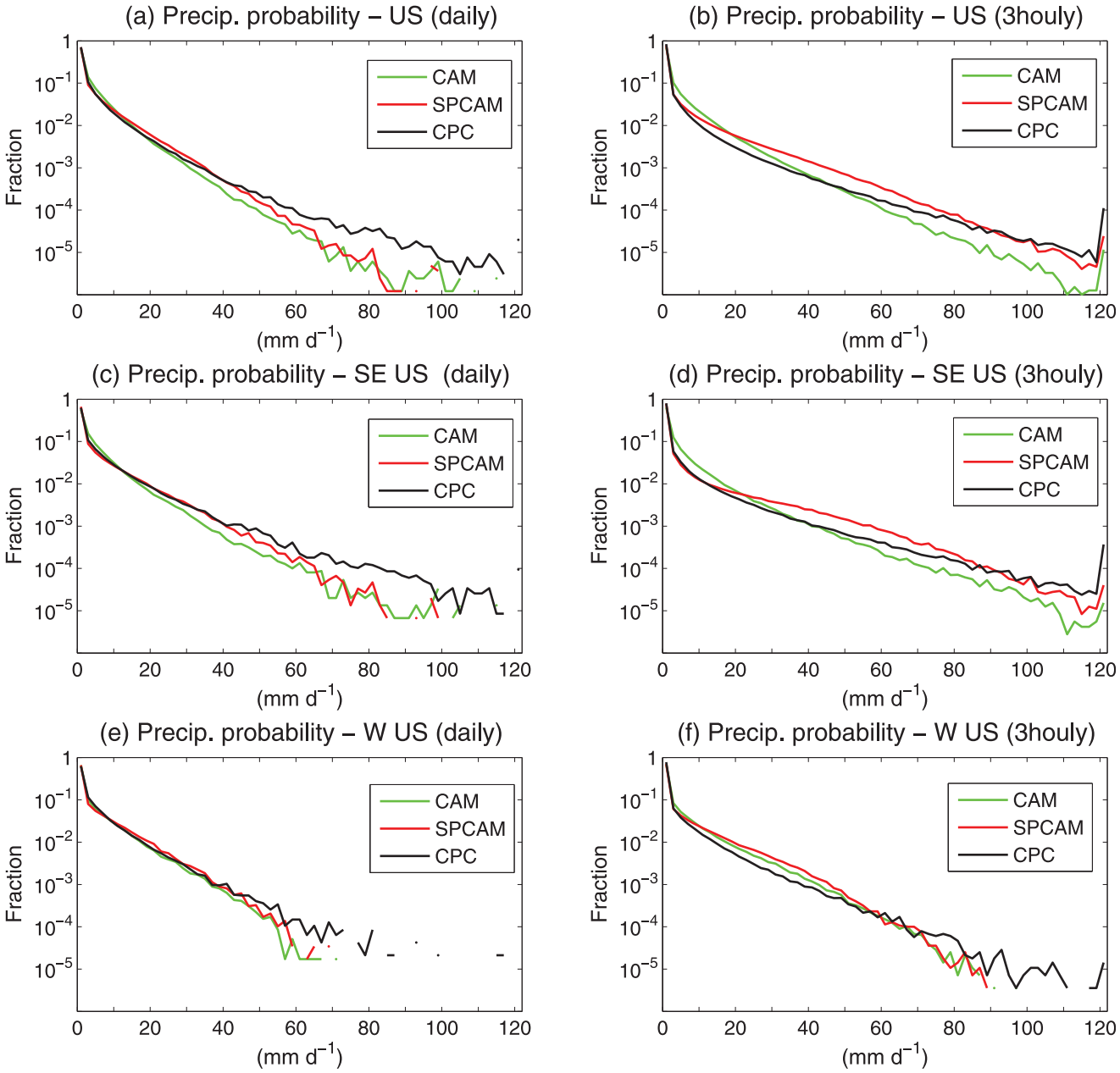

Figure 4. Probability density distributions of (a) U.S. daily precipitation; (b) U.S. 3-hourly precipitation; (c) southeastern (SE) U.S. daily precipitation; (d) southeastern (SE) U.S. 3-hourly precipitation; (e) western (W) U.S. daily precipitation; and (f) western (W) U.S. 3-hourly precipitation. Green, red, and black lines respectively represent the CAM, SP-CAM, and CPC.

the CAM simulated summertime precipitation probability distribution differs appreciably from the CPC distribution. Again, SP-CAM offers significant improvements over CAM. Although it overestimates the moderate precipitation, it captures the higher end of the distribution very well (Figure 5b). These results suggest SP-CAM appears to have better fidelity to the observational record for both light and extreme precipitation during the convective precipitation dominated season. As for the daily precipitation distribution, the differences between CAM and SP-CAM 3-hourly distributions are small for the winter season when large-scale precipitation predominates. Both models simulate the observed distribution with comparable levels of accuracy (Figure 5d).

3.4. The Roles of Cloud Physics and Dynamics in Inter-model Differences

[26] Differences in large-scale dynamic and thermodynamic fields cannot cause the differences in extreme precipitation simulated by CAM and SP-CAM since these fields are constrained by the same NCEP-reanalysis data at each model time step and are therefore almost identical in our two simulations.

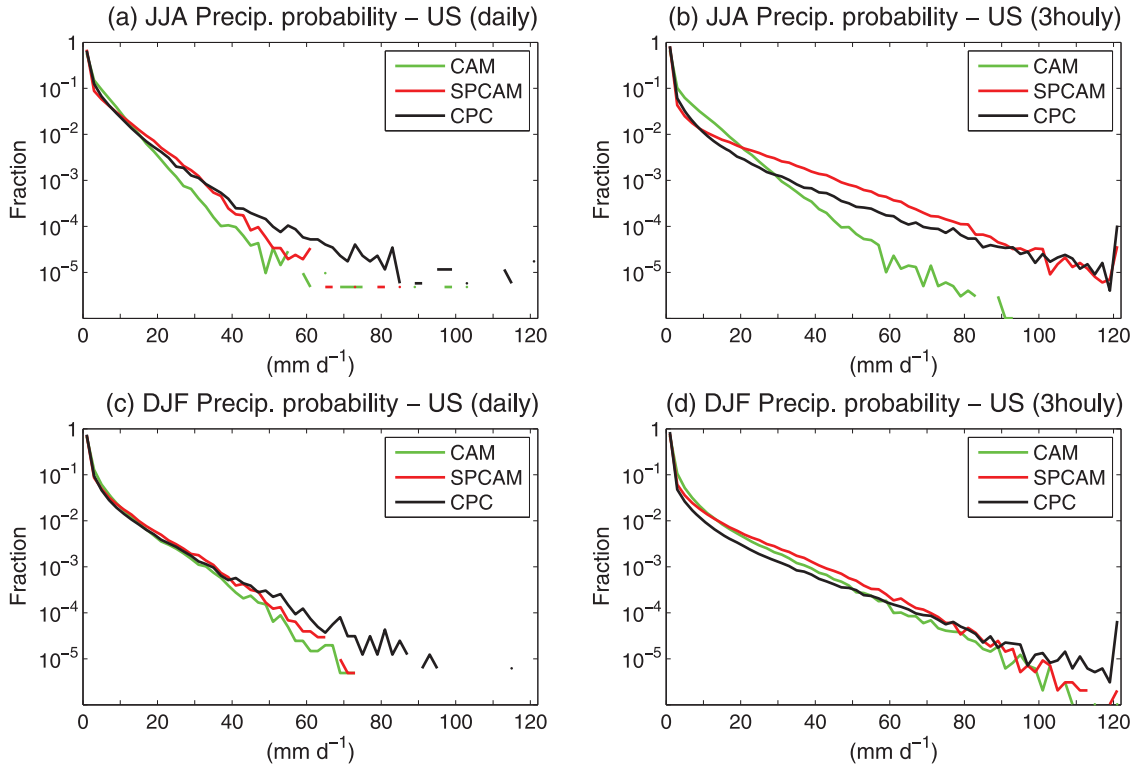

Figure 5. Probability density distributions of (a) JJA U.S. daily precipitation; (b) JJA U.S. 3-hourly precipitation; (c) DJF daily precipitation; and (d) DJF 3hourly precipitation.

Instead, the differences can be attributed to some combination of three main subgrid-scale processes: (1) the advection of water vapor to altitudes above its lifted condensation level (LCL) in convective updrafts; (2) the condensation of the resulting supersaturated vapor to form cloud water and ice; and (3) the conversion of this cloud condensate to precipitation. The first process is governed primarily by rates of subgrid vertical advection and the latter two are determined by cloud microphysical processes for condensation and collisional coalescence. An assessment of which of the three subgrid processes explains the different statistics of extreme precipitation in CAM and SP-CAM would provide insights into how best to improve the simulation of cloud and precipitation in climate models.

[27] Due to the challenges posed by retrospective analysis of the sub-grid physics and parameterizations and due to the absence of suitable run-time diagnostics, we do not have sufficient information to individually quantify the differences in the first two processes associated with moisture lifting or cloud condensation. Their combined effects, however, are reflected in the total cloud water produced by CAM and SP-CAM. The third process, e.g., conversion from cloud water to precipitation, can be quantified using a precipitation efficiency f defined as the ratio of precipitation rate to the total grid box cloud water path. The parameter f has units of 1/days and represents the inverse timescale for the conversion of cloud condensate to precipitation. Hence larger values of f correspond to shorter timescales for the conversion process.

[28] The total cloud condensate path and total precipitation amount for all the summer precipitation events are shown in Figures 6a and 6b, respectively. The 80 mm d^{-1} upper boundary is chosen since there is almost no precipitation larger than 80 mm d^{-1} in CAM. We accumulate all the precipitation events falling into a given precipitation bin to obtain the total amounts of cloud condensate and precipitation. The efficiency f for each bin is estimated by dividing the total precipitation amount by the corresponding total cloud condensate path.

[29] The total cloud condensate in SP-CAM is much higher than the condensate in CAM for heavy precipitation events. The condensate paths in SP-CAM are almost two orders of magnitude higher than those in CAM at precipitation rates approaching 80 mm d^{-1} (Figure 6a). The magnitude of this difference corresponds well with the magnitude of differences in the precipitation amount (Figure 6b) and probability distribution (Figure 5b). In addition, the precipitation efficiency of SP-CAM exceeds that in CAM by approximately 20% for all precipitation intensities higher than 30 mm d^{-1} (Figure 6c). This shows that the microphysics for the conversion of cloud condensate to hydrometeors in SP-CAM produces precipitation 20% faster than the corresponding parameterizations in CAM given identical amounts of cloud water in the two models. However, the magnitude of this difference in conversion rates is one to two orders of magnitude smaller than the total differences in extreme precipitation. These results suggest that improvements in extreme

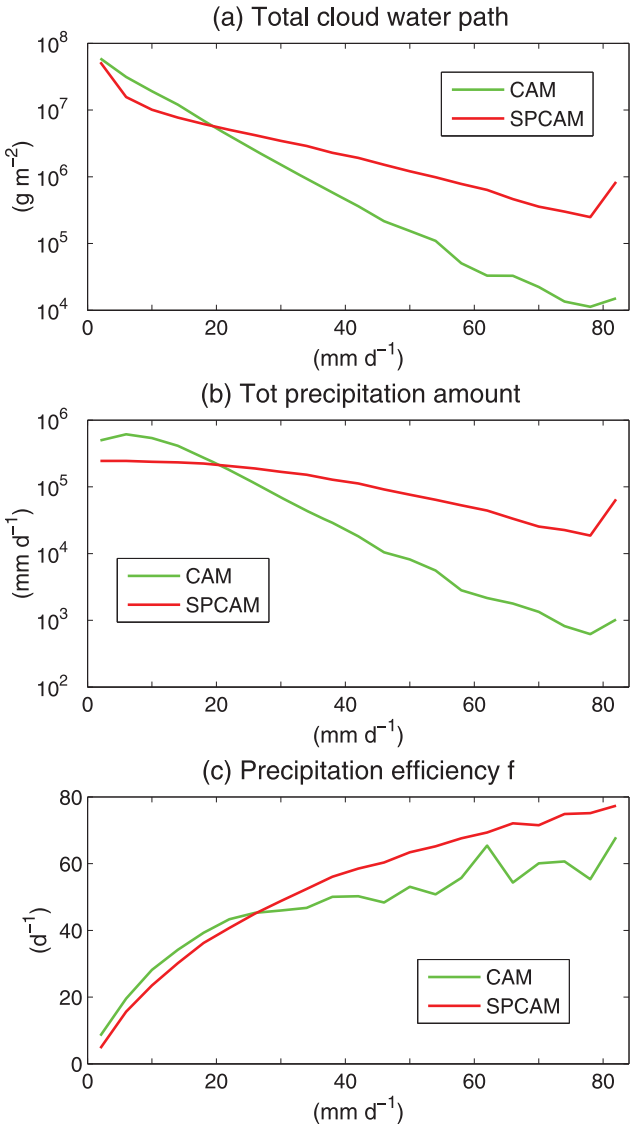

Figure 6. (a) Total could water path and (b) total precipitation amount, accumulated in 4 mm d-1 precipitation intensity bins, for all the 3-hourly precipitation events during JJA from 1996 to 2001 over CONUS. (c) Precipitation efficiency f = precipitation rate / total grid box cloud water path.

precipitation simulated by SP-CAM are caused primarily by differences in the representation of moisture advection and cloud condensation, the two remaining subgrid processes. In particular, the moisture-advection process is fundamentally different in CAM and SP-CAM since the bulk of vertical water transport is due to small-scale circulations explicitly represented on each CRM's grid.

4. Conclusion and Discussion

[30] This study has evaluated a new approach for simulating extreme precipitation over large spatial scales based upon replacing conventional parameterizations with CRMs in a global GCM. We perform two experiments to evaluate this approach contrasting the standard Community Atmosphere Model (CAM) and a "super-parameterized" CAM (SP-CAM) with the grid-scale tendencies in both experiments constrained by identical NCEP reanalysis fields. Under this framework, the differences between the two experiments are solely due to differences in subgrid process representations between CAM and SP-CAM. While cloud microphysical processes are parameterized in both models, convective updrafts and downdrafts are explicitly resolved in SP-CAM at the resolution of the embedded CRMs. Gridded estimates of U.S. precipitation derived by the CPC from rain gauge data are used to evaluate the simulated statistics of extreme precipitation.

[31] Our results show that more extreme precipitation is simulated by SP-CAM than by CAM over almost all the CONUS region despite the fact that both models simulate very similar distributions of mean precipitation. Compared to the CPC estimates, SP-CAM is much better agreement than CAM in both the spatial distribution and intensity of extreme precipitation, especially at very high rain rates (99.5% percentile) and short (3-hourly) time scales. While the underestimation of extreme precipitation by CAM, as well as other GCMs, has been previously reported [e.g., *Boyle and Klein*, 2010; *Li et al.*, 2011b], it is encouraging to see the improvement with the implementation of CRM.

[32] A closer look at the probability distribution of the precipitation shows that the distribution produced by SP-CAM generally agrees with the CPC observations better than that produced by CAM. SP-CAM simulates more light precipitation and more heavy precipitation and this improvement is especially pronounced at 3-hourly time scales, although the ability of SP-CAM to simulate very extreme precipitation (e.g., daily rates in excess 60 mm d^{-1}) remains limited.

[33] Distinct differences in the CAM and SP-CAM simulations are found in the two regions with the most extreme precipitation: the southeastern U.S. and the western coastal US. Over the southeastern US, SP-CAM agrees considerably better with the CPC in the distribution of precipitation than CAM at both the daily and 3-hourly time scales. However, the difference between CAM, SP-CAM, and CPC is much smaller at both of these time scales in the western coastal US. Since convective processes are a more important source of extreme precipitation in the southeastern U.S. while the extreme rainfall in the western coastal U.S. is largely due to large scale air motions, these regional differences imply that improvements obtained with SP-CAM are due primarily to the enhanced treatment of subgrid-scale convective processes. The seasonal variation of the precipitation distribution confirms that convective processes are the key in improvement of SP-CAM over CAM. During the convective dominated summer season, SP-CAM clearly outperforms CAM, particularly at 3-hourly time scales. The summertime precipitation distribution simulated by CAM is clearly less realistic than that simulated by SP-CAM. This validates the expectation that the subgrid convective processes, not the large-scale air motions, are better represented by the SP-CAM.

[34] The subgrid dynamics and physics are purported to be better resolved at the cloud scale and hence potentially more realistic in SP-CAM, Several subgrid processes could potentially result in the more extreme precipitation produced by SP-CAM, including moisture advection, cloud condensation, and the conversion from cloud water to precipitation. We show that SP-CAM has somewhat higher cloud-water-to-precipitation conversion efficiency than CAM for moderate to high precipitation and that the greater efficiency contributes to some of the improvement of SP-CAM in simulating extreme precipitation. However, the major difference between CAM and SP-CAM is due to SP-CAM's ability to produce much more cloud water during the heavy precipitation events, although we are not able to quantify the relative importance of moisture advection and cloud condensation in the cloud condensate production in the current experiments.

[35] Bridging between conventional GCMs and global scale CRMs, SP-CAM appears to be a new promising approach of simulating and projecting the changes and trends of extreme precipitation in regions of the world where convective processes are significant. With the increased availability of computation resources, more tests and assessments of SP GCMs or ultimately global-scale CRMs should be carried out and the results would provide key information to improve the physical representations of extreme precipitation in the models for robust simulations and projections.

[36] **Acknowledgments.** This work was supported by the Director, Office of Science, Office of Biological and Environmental Research, Climate Change Research Division, of the U.S. Department of Energy under Contract No. DE-AC02-05CH11231. CPC US Unified Precipitation data provided by the NOAA/OAR/ESRL PSD, Boulder, Colorado, USA, from their Web site at http://www.esrl.noaa.gov/psd/. Computational resources were obtained from the National Energy Research Scientific Computing Center (NERSC).

References

Alexander, L. V., et al. (2006), Global observed changes in daily climate extremes of temperature and precipitation, *J. Geophys. Res.*, *111*, D05109, doi:10.1029/2005JD006290.

Boyle, J., and S. A. Klein (2010), Impact of horizontal resolution on climate model forecasts of tropical precipitation and diabatic heating for the TWP-ICE period, *J. Geophys. Res.*, *115*, D23113, doi:10.1029/2010JD014262.

Charba, J. P., A. W. Harrell III, and A. C. Lackner III (1992), A monthly precipitation amount climatology derived from published atlas maps: Development of a digital data base, *TDL Off. Note 92-7*, 20 pp., U.S. Dep. of Commer., Washington, D. C.

Chen, C. T., and T. Knutson (2008), On the verification and comparison of extreme rainfall indices from climate models, *J. Clim.*, *21*, 1605–1621, doi:10.1175/2007JCLI1494.1.

Collins, W. D., et al. (2004), Description of the NCAR Community Atmosphere Model (CAM3), *Tech. Note NCAR-TN-464+STR*, Natl. Cent. for Atmos. Res., Boulder, Colo.

Collins, W. D., et al. (2006), The formulation and atmospheric simulation of the Community Atmospheric Model: CAM3, *J. Clim.*, *19*, 2144–2161, doi:10.1175/JCLI3760.1.

Cressman, G. P. (1959), An operational objective analysis system, *Mon. Weather Rev.*, *87*, 367–374, doi:10.1175/1520-0493(1959)087<0367:AOOAS>2.0.CO;2.

DeMott, C. A., D. A. Randall, and M. Khairoutdinov (2007), Convective precipitation variability as a tool for general circulation model analysis, *J. Clim.*, *20*, 91–112, doi:10.1175/JCLI3991.1.

Durman, C. F., J. M. Gregory, D. C. Hassell, R. G. Jones, and J. M. Murphy (2001), Comparison of extreme European daily precipitation simulated by a global and a regional climate model for present and future climates, *Q. J. R. Meteorol. Soc.*, *127*, 1005–1015, doi:10.1002/qj.49712757316.

Frich, P., et al. (2002), Observed coherent changes in climatic extremes during the second half of the twentieth century, *Clim. Res.*, *19*, 193–212, doi:10.3354/cr019193.

Higgins, R. W., W. Shi, E. Yarosh, and R. Joyce 2000, Improved United States precipitation quality control system and analysis, *NCEP/Climate Prediction Center ATLAS No. 7*, 40 pp., Camp Springs, Md.

Iorio, J. P., P. B. Duffy, B. Govindasamy, S. L. Thompson, M. Khairoutdinov, and D. Randall (2004), Effects of model resolution and subgrid-scale physics on the simulation of precipitation in the continental United States, *Clim. Dyn.*, *23*, 243–258, doi:10.1007/s00382-004-0440-y.

Kalnay, E., et al. (1996), The NCEP/NCAR 40-year reanalysis project, *Bull. Am. Meteorol. Soc.*, *77*, 437–471, doi:10.1175/1520-0477(1996)077<0437:TNYRP>2.0.CO;2.

Khairoutdinov, M. F., and D. A. Randall (2001), A cloud resolving model as a cloud parameterization in the NCAR Community Climate System Model: Preliminary results, *Geophys. Res. Lett.*, *28*, 3617–3620, doi:10.1029/2001GL013552.

Khairoutdinov, M. F., D. A. Randall, and C. DeMott (2005), Simulations of the atmospheric general circulation using a cloud-resolving model as a super- parameterization of physical processes, *J. Atmos. Sci.*, *62*, 2136–2154, doi:10.1175/JAS3453.1.

Khairoutdinov, M., C. DeMott, and D. Randall (2008), Evaluation of the simulated interannual and subseasonal variability in an AMIP-style simulation using the CSU Multiscale Modeling Framework, *J. Clim.*, *21*, 413–431, doi:10.1175/2007JCLI1630.1.

Li, F., W. D. Collins, M. F. Wehner, D. L. Williamson, and J. G. Olson (2011a), Response of precipitation extremes to global warming in an aqua-planet climate model: towards robust projection from regional to global scales, *Tellus, Ser. A*, *63*(5), 876–883, doi:10.1111/j.1600-0870.2011.00543.x.

Li, F., W. D. Collins, M. F. Wehner, D. L. Williamson, J. G. Olson, and C. Algieri (2011b), Impact of horizontal resolution on simulation of precipitation extremes in an aqua-planet version of the Community Atmosphere Model (CAM), *Tellus, Ser. A*, *63*(5), 884–892, doi:10.1111/j.1600-0870.2011.00544.x.

Min, S.-K., X. B. Zhang, F. W. Zwiers, P. Friederichs, and A. Hense (2009), Signal detectability in extreme precipitation changes assessed from twentieth century climate simulations, *Clim. Dyn.*, *32*, 95–111, doi:10.1007/s00382-008-0376-8.

Min, S.-K., X. Zhang, F. W. Zwiers, and G. C. Hegerl (2011), Human contribution to more-intense precipitation extremes, *Nature*, *470*, 378–381, doi:10.1038/nature09763.

Ooyama, K. V. (2001), A dynamic and thermodynamic foundation for modeling the moist atmosphere with parameterized microphysics, *J. Atmos. Sci.*, *58*, 2073–2102, doi:10.1175/1520-0469(2001)058<2073:ADATFF>2.0.CO;2.

Schneider, S. H., et al. (2007), Assessing key vulnerabilities and the risk from climate change, in *Climate Change 2007: Impacts, Adaptation and Vulnerability. Contribution of Working Group II to the Fourth Assessment Report of the Intergovernmental Panel on Climate Change*, edited by M. L. Parry et al., pp. 779–810, Cambridge Univ. Press, Cambridge, U. K.

Wehner, M. F., R. Smith, P. Duffy, and G. Bala (2010), The effect of horizontal resolution on simulation of very extreme U.S. precipitation events in a global atmosphere model, *Clim. Dyn.*, *34*, 241–247, doi:10.1007/s00382-009-0656-y.

Williamson, D. L. (2008), Convergence of aqua-planet simulations with increasing resolution in the Community Atmospheric Model, Version 3, *Tellus, Ser. A*, *60*(5), 848–862, doi:10.1111/j.1600-0870.2008.00339.x.

W. D. Collins and F. Li, Earth Sciences Division, Lawrence Berkeley National Laboratory, 1 Cyclotron Rd., Berkeley, CA 94720, USA. (fli@lbl.gov)

D. Rosa, Department of Earth and Planetary Science, University of California, Berkeley, CA 94720, USA.

M. F. Wehner, Computational Research Division, Lawrence Berkeley National Laboratory, Berkeley, CA 94720, USA.